

Magnetic and pairing properties of a two-orbital model for the pnictide superconductors: A quantum Monte Carlo study

Guang-Kun Liu,^{1,*} Zhong-Bing Huang,^{2,3,†} and Yong-Jun Wang^{1,‡}

¹*Department of Physics, Beijing Normal University, Beijing 100875, China*

²*Department of Physics, Hubei University, Wuhan 430062, China*

³*Beijing Computational Science Research Center, Beijing 100084, China*

(Dated: February 20, 2014)

Using the constrained-path Monte Carlo method, a two-orbital model for the pnictide superconductors is studied at half filling and in both the electron- and hole-doped cases. At half filling, a stable $(\pi, 0)/(0, \pi)$ magnetic order is explicitly observed, and the system tends to be in an orthomagnetic order rather than the striped antiferromagnetic order when increasing the Coulomb repulsion U . In the electron-doped case, the $(\pi, 0)/(0, \pi)$ magnetic order is enhanced upon doping and suppressed eventually, and a s_{\pm} pairing state dominates all the possible nearest-neighbor-bond pairings. Whereas in the hole-doped case, the magnetic order is straightforwardly suppressed and two nearly degenerate A_{1g} and B_{1g} intraband pairings become the dominant ones.

PACS numbers: 71.10.Fd, 74.20.Rp, 74.70.Xa, 74.20.Mn

I. INTRODUCTION

The discovery of pnictide superconductors (SCs) has triggered lots of attentions of the condensed matter community. Unlike cuprates, where only the Cu $3d_{x^2-y^2}$ orbital plays the most significant role, the local-density approximation (LDA) calculations^{1,2} indicate that pnictide SCs have several active $3d$ orbitals near the Fermi surface (FS). Consequently, it is widely believed that such SCs should be understood in terms of multi-orbital models instead of the single-orbital ones.³⁻⁵ Regarding the minimal model capable of capturing the essential physics of pnictide SCs, some authors proposed more realistic three- and five-orbital models,^{4,5} while others argued that the main physics of the pnictide SCs are contained in two-orbital models.^{3,6,7} Because of their relative simplicity, as well as the fact that⁶ the correct FS shape can be reproduced in both the doped and undoped cases, it is crucial to find out the properties of these two-orbital models.

Most previous theoretical works on the two-orbital models for pnictides were based on mean-field-like approximations, such as the random phase approximation (RPA), fluctuation exchange (FLEX) and functional renormalization group (fRG) calculations and so on. The main results from these studies provided good understandings of pnictides while still giving very different pairing pictures. For instance, Graser *et al.* proposed two nearly degenerate competing pairing states with A_{1g} and B_{1g} symmetries because of the near nesting of FS sheets.⁸ Although other RPA studies also suggested a competing pairing picture, different pairing channels were proposed, for example, the competition between singlet d -wave and triplet p -wave states⁹ or s_{\pm} -wave and d -wave states.¹⁰ Aside from RPA studies, a FLEX calculation demonstrated an s_{\pm} -wave or d_{xy} -wave pairing depending on whether the intraband antiferromagnetic (AFM) spin fluctuation is stronger than the interband one or not¹¹. Meanwhile, fRG approach revealed s_{\pm} -wave and sub-

dominant d -wave pairings.¹² Moreover, Dai *et al.* suggested a spin triplet pairing state by using of the BCS mean field method.¹³

From the above discussions, it seems of great difficulty to justify the pairing symmetry of the two-orbital models. Since it is unrealistic to take the full quantum fluctuations into account in the usual theoretical methods, the important role of electronic correlations on the magnetism and superconductivity has not been thoroughly recognized. Despite the fact that there exist some unbiased numerical investigations of the two-orbital model,^{6,14-16} these results are not sufficient enough to understand the electronic correlations in the two-dimensional systems because they are obtained either on a 8-site lattice^{6,14,15} or on a diagonal ladder.¹⁶ For a comprehensive and systematic understanding of the two-orbital model,^{3,14} a quantum Monte Carlo (QMC) method is employed in this paper.

However, it is known that there are several difficulties in the QMC simulations of the two-orbital models: One is the severe limitation of the cluster size. For example, the computational demanding of a two-orbital model with a given cluster is much higher than that of an one-orbital model with a double cluster size. Another^{17,18}, probably the most tough one, is the insurmountable Fermi sign problem. Compared to the one-orbital model, a usual discrete Hubbard-Stratonovich (HS) transformation¹⁹ for the Hund's coupling and pair-hopping terms, which is specific to the multi-orbital models, does lead to a more serious sign problem. It is noticed that Sakai *et al.*¹⁸ proposed a new type of transformation for the Hund's coupling and pair-hopping interaction, which can effectively alleviate the sign problem. Based on this progress, we developed a feasible constrained-path Monte Carlo (CPMC) method²⁰ for the two-orbital models, which works well in the weak and intermediate correlation regimes.

Using the CPMC method, we compute the magnetic structure factors and the pairing correlations of the two-

orbital model as functions of the doping density ρ and interaction strength U . We find a $(\pi, 0)/(0, \pi)$ magnetic order that is enhanced by the Coulomb repulsion U and the Hund's coupling J in the undoped case. Because of the particle-hole asymmetry of the two-orbital model, such a magnetic order shows different behaviors in the electron- and hole-doped cases. We also find that the doping has much stronger effect than that of the Coulomb repulsion on the pairing correlations. In the electron-doped case, a nodeless s_{\pm} pairing is dominant, whereas in the hole-doped case, two nearly degenerate A_{1g} and B_{1g} intraband singlet pairings compete with each other and become the dominant ones.

Our paper is organized as follows: In Sec. II, we briefly introduce the two-orbital model under investigation and discuss the proper choice of model parameters. Some modifications to the original CPMC algorithm and the definitions of the calculated physical quantities are presented as well. In Sec. III, we exhibit in details the simulation results for the magnetic and pairing properties of the model with various parameters. Our main conclusions are summarized in Sec. IV.

II. MODEL AND NUMERICAL APPROACH

On the basis of LDA calculations, Mazin *et al.*² advocated that the band structure of pnictides involves only three Fe 3d orbitals, d_{xz} , d_{yz} , and d_{xy} (or $d_{x^2-y^2}$), near the Fermi level. Accordingly, Raghu *et al.*³ introduced a minimal multi-orbital model for the pnictide SCs within the further approximation that a next-near-neighbor hybridization between d_{xz} , d_{yz} orbitals can be equated to the role of the d_{xy} or $d_{x^2-y^2}$ orbital. As described in Ref. 14, the kinetic part of the two-orbital model Hamiltonian is given by

$$\begin{aligned} H_0 = & -t_1 \sum_{\mathbf{i}, \sigma} (d_{\mathbf{i}, x, \sigma}^\dagger d_{\mathbf{i}+\hat{x}, y, \sigma} + d_{\mathbf{i}, y, \sigma}^\dagger d_{\mathbf{i}+\hat{x}, x, \sigma} + \text{h.c.}) \\ & -t_2 \sum_{\mathbf{i}, \sigma} (d_{\mathbf{i}, x, \sigma}^\dagger d_{\mathbf{i}+\hat{x}, x, \sigma} + d_{\mathbf{i}, y, \sigma}^\dagger d_{\mathbf{i}+\hat{y}, y, \sigma} + \text{h.c.}) \\ & -t_3 \sum_{\mathbf{i}, \hat{\mu}, \hat{\nu}, \sigma} (d_{\mathbf{i}, x, \sigma}^\dagger d_{\mathbf{i}+\hat{\mu}+\hat{\nu}, x, \sigma} + d_{\mathbf{i}, y, \sigma}^\dagger d_{\mathbf{i}+\hat{\mu}+\hat{\nu}, y, \sigma} + \text{h.c.}) \\ & +t_4 \sum_{\mathbf{i}, \sigma} (d_{\mathbf{i}, x, \sigma}^\dagger d_{\mathbf{i}+\hat{x}+\hat{y}, y, \sigma} + d_{\mathbf{i}, y, \sigma}^\dagger d_{\mathbf{i}+\hat{x}+\hat{y}, x, \sigma} + \text{h.c.}) \\ & -t_4 \sum_{\mathbf{i}, \sigma} (d_{\mathbf{i}, x, \sigma}^\dagger d_{\mathbf{i}+\hat{x}-\hat{y}, y, \sigma} + d_{\mathbf{i}, y, \sigma}^\dagger d_{\mathbf{i}+\hat{x}-\hat{y}, x, \sigma} + \text{h.c.}) \end{aligned} \quad (1)$$

where x and y represent the d_{xz} and d_{yz} orbitals, respectively. The operator $d_{\mathbf{i}\alpha\sigma}^\dagger$ creates an electron on orbital α in Fe site \mathbf{i} with spin σ , and the index $\hat{\mu}(\hat{\nu}) = \hat{x}$ or \hat{y} denotes a unit vector linking the nearest-neighbor sites. To estimate the hopping amplitudes that can recover the right topology of Fermi surface and band features given by DFT,^{21,22} the band-structure calculation³ and the Slater-Koster tight-binding scheme⁶ recommended different hopping amplitudes, however, the Lanczos study on

8-site cluster suggested these two schemes give similar physics⁶. Following the band-structure calculation, the hopping parameters will always be taken as $t_1 = -1.0$, $t_2 = 1.3$ and $t_3 = t_4 = -0.85$ in our calculation.

The interaction terms,^{14,23,24} containing a Hubbard repulsion in the same orbital, a repulsion U' for different orbitals, a ferromagnetic Hund's coupling J , and pair-hopping terms, can be expressed as

$$\begin{aligned} H_{int} = & \sum_{\mathbf{i}} (H_1^{\mathbf{i}} + H_2^{\mathbf{i}} + H_3^{\mathbf{i}} + H_4^{\mathbf{i}}), \\ H_1^{\mathbf{i}} = & J \sum_{\alpha \neq \alpha'} (d_{\mathbf{i}\alpha\uparrow}^\dagger d_{\mathbf{i}\alpha'\downarrow}^\dagger d_{\mathbf{i}\alpha\downarrow} d_{\mathbf{i}\alpha'\uparrow} \\ & + d_{\mathbf{i}\alpha\uparrow}^\dagger d_{\mathbf{i}\alpha\downarrow}^\dagger d_{\mathbf{i}\alpha'\downarrow} d_{\mathbf{i}\alpha'\uparrow}), \\ H_2^{\mathbf{i}} = & (U' - J) \sum_{\sigma} n_{\mathbf{i}, x, \sigma} n_{\mathbf{i}, y, \sigma}, \\ H_3^{\mathbf{i}} = & U \sum_{\alpha} n_{\mathbf{i}\alpha\uparrow} n_{\mathbf{i}\alpha\downarrow}, \\ H_4^{\mathbf{i}} = & U' \sum_{\sigma} n_{\mathbf{i}, x, \sigma} n_{\mathbf{i}, y, -\sigma}, \end{aligned} \quad (2)$$

where α denotes the d_{xz} or d_{yz} orbital and U' satisfies the constraint $U' = U - 2J$ due to the rotational invariance.²⁵ Throughout this work, the correlation strength is taken up to the intermediate range, i.e., $U/|t_1| \lesssim 2$ for both undoped and doped cases, which is believed to be proper for the pnictides SCs.²⁶

In Eq. (2), $H_1^{\mathbf{i}}$ can be transformed¹⁸ as

$$e^{-\Delta\tau H_1^{\mathbf{i}}} = \frac{1}{2} \sum_{\gamma=\pm 1} e^{\lambda\gamma(f_{\mathbf{i}\uparrow} - f_{\mathbf{i}\downarrow})} e^{a(N_{\mathbf{i}\uparrow} + N_{\mathbf{i}\downarrow}) + bN_{\mathbf{i}\uparrow}N_{\mathbf{i}\downarrow}} \quad (3)$$

with

$$\begin{aligned} f_{\mathbf{i}, \sigma} = & d_{\mathbf{i}, x, \sigma}^\dagger d_{\mathbf{i}, y, \sigma} + d_{\mathbf{i}, y, \sigma}^\dagger d_{\mathbf{i}, x, \sigma}, \\ N_{\mathbf{i}, \sigma} = & n_{\mathbf{i}, x, \sigma} + n_{\mathbf{i}, y, \sigma} - 2n_{\mathbf{i}, x, \sigma} n_{\mathbf{i}, y, \sigma}, \end{aligned} \quad (4)$$

where a , b and λ are some parameters depending on Hund's coupling J and Trotter interval $\Delta\tau$, and $\gamma = \pm 1$ is the newly introduced auxiliary field.

Due to the property that $N_{\mathbf{i}, \sigma}^2 = N_{\mathbf{i}, \sigma}$, the factor $e^{bN_{\mathbf{i}\uparrow}N_{\mathbf{i}\downarrow}}$ in Eq. (3) can be further decoupled into a product of single $e^{N_{\mathbf{i}\sigma}}$ -like terms using the discrete HS transformation¹⁹. Then all the terms containing $e^{N_{\mathbf{i}\sigma}}$, which are independent of the introduced field γ in Eq. (3), can be combined with $H_2^{\mathbf{i}}$ in Eq. (2) for the ordinary CPMC treatment. However, after this recombination, we can see that the remaining factor in Eq.(3), $e^{\lambda\gamma(f_{\mathbf{i}\uparrow} - f_{\mathbf{i}\downarrow})}$, contrary to other interactions which are made up of the number operator $n_{\mathbf{i}, \alpha, \sigma}$, involves some hopping-like terms. So some adjustment must be made for this new item $e^{\lambda\gamma(f_{\mathbf{i}\uparrow} - f_{\mathbf{i}\downarrow})}$.

Recalling that in the standard QMC algorithm, the matrix form of the interaction term, such as the Hubbard repulsion $H_1^{\mathbf{i}}$, always has the form:

$$e^{H_1^{\mathbf{i}}} = I + A, \quad (5)$$

where A is sparse with one element in the diagonal and I is the identity matrix. Consequently, the determinant division $\frac{\det L(I+A)R}{\det LR}$ and the matrix inverse $(L(I+A)R)^{-1}$ can be calculated using a fast updating algorithm.^{27,28}

We find that the matrix form of $e^{\lambda\gamma f_{i\sigma}} = e^{\lambda\gamma(d_{i,x,\sigma}^\dagger d_{i,y,\sigma} + \text{h.c.})}$ can be cast into a similar form as Eq. (5):

$$e^{\lambda\gamma(d_{i,x,\sigma}^\dagger d_{i,y,\sigma} + \text{h.c.})} = I + B \quad (6)$$

but with B having four non-zero elements

$$B = \begin{pmatrix} \ddots & & & & \\ & b_{mm} & \cdots & b_{mn} & \\ & \vdots & \ddots & \vdots & \\ & b_{nm} & \cdots & b_{nn} & \\ & & & & \ddots \end{pmatrix}, \quad (7)$$

where $b_{mm} = b_{nn} = \frac{e^{-\lambda\gamma} + e^{\lambda\gamma}}{2} - 1$, $b_{mn} = b_{nm} = \frac{-e^{-\lambda\gamma} + e^{\lambda\gamma}}{2}$. If we insert the unitary matrix $UU^{-1}(I+B)UU^{-1}$ to make $U^{-1}(I+B)U = I+B'$ with B' the desired diagonal form as A in Eq. (5), the determinant division $\frac{\det L(I+B)R}{\det LR}$ and the matrix inverse $(L(I+B)R)^{-1}$ can then be written as

$$\frac{\det L(I+B)R}{\det LR} = \frac{\det L'(I+B')R'}{\det LR}, \quad (8)$$

$$(L(I+B)R)^{-1} = (L'(I+B')R')^{-1},$$

where $L' = LU$ and $R' = U^{-1}R$. Now the standard CPMC algorithm can be applied with the new formulas of Eq. (8).

In order to investigate the magnetic properties, we examine the magnetic correlations through the static magnetic structure factor

$$S(k) = 1/N \sum_{ij} e^{i\mathbf{k} \cdot (\mathbf{r}_i - \mathbf{r}_j)} \langle (n_{i\uparrow} - n_{i\downarrow})(n_{j\uparrow} - n_{j\downarrow}) \rangle, \quad (9)$$

where $n_{i\sigma} = n_{i,x,\sigma} + n_{i,y,\sigma}$.

Concerning the pairing properties, the classification of possible pairing symmetries in Ref. 29 is followed (see Table. I). In the multi-orbital systems, the pairing operators have both spatial and orbital degrees of freedom.³⁰ The singlet and triplet (with projection 1) pairing operators, $\Delta_s^\dagger(\mathbf{k})$ and $\Delta_t^\dagger(\mathbf{k})$, can be respectively defined as

$$\Delta_s^\dagger(\mathbf{k}) = \frac{1}{\sqrt{2}} f(\mathbf{k})(\tau_i)_{\alpha,\beta} (d_{\mathbf{k},\alpha,\uparrow}^\dagger d_{-\mathbf{k},\beta,\downarrow}^\dagger - d_{\mathbf{k},\alpha,\downarrow}^\dagger d_{-\mathbf{k},\beta,\uparrow}^\dagger),$$

$$\Delta_t^\dagger(\mathbf{k}) = f(\mathbf{k})(\tau_i)_{\alpha,\beta} d_{\mathbf{k},\alpha,\uparrow}^\dagger d_{-\mathbf{k},\beta,\uparrow}^\dagger,$$

where $d_{\mathbf{k},\alpha,\sigma}^\dagger$ creates an electron in orbital α with momentum \mathbf{k} and spin σ , and $f(\mathbf{k})$ is the form factor that transforms according to one of the irreducible representations of the symmetry group³⁰ (for concrete forms see Table. I), while τ_i 's are the Pauli matrices ($i = 1, 2, 3$) or

TABLE I: The possible nearest-neighbor-bond pairing basis matrices of the two-orbital models used in our simulations (Ref. 29). The first column is the index number, the second and third columns list the representations and the basis matrices $f(\mathbf{k})\tau_i$. The last column shows the spin parities where S refer to singlet and T to triplet. Note that a nodeless s_\pm is also listed in the first row.

No.	IR	$f(\mathbf{k})\tau_i$	Spin
s_\pm	A_{1g}	$\cos k_x \cos k_y \tau_0$	S
2	A_{1g}	$(\cos k_x + \cos k_y) \tau_0$	S
3	A_{1g}	$(\cos k_x - \cos k_y) \tau_0$	S
4	A_{2g}	$(\cos k_x - \cos k_y) \tau_1$	S
6	B_{1g}	$(\cos k_x - \cos k_y) \tau_0$	S
7	B_{1g}	$(\cos k_x + \cos k_y) \tau_3$	S
9	B_{2g}	$(\cos k_x + \cos k_y) \tau_1$	S
10	E_g	$\sin k_x i \tau_2$	S
12	A_{2g}	$(\cos k_x + \cos k_y) i \tau_2$	T
13	B_{2g}	$(\cos k_x - \cos k_y) i \tau_2$	T
14	E_g	$\sin k_x \tau_0$	T
15	E_g	$\sin k_x \tau_3$	T
16	E_g	$\sin k_x \tau_1$	T

identity matrix ($i = 0$). Using the Fourier transformation, we can get the pairing operator in coordinate space $\Delta(\mathbf{i})$, and the corresponding pairing correlation function is defined as

$$P(r = |\mathbf{i} - \mathbf{j}|) = \langle \Delta^\dagger(\mathbf{i}) \Delta(\mathbf{j}) \rangle. \quad (10)$$

Our CPMC code is checked by comparing to the Lanczos results on the 2×2 and 3×2 clusters and also to a previous 8-site cluster Lanczos simulation⁶. Our CPMC data are completely consistent with those results.

III. RESULTS AND DISCUSSIONS

A. Magnetic property

First we discuss the magnetic order in the undoped system. As shown in Fig. 1(a), the magnetic structure factor $S(k)$ is presented at half filling (one electron per orbital) for different Coulomb repulsions U and Hund's couplings J on the 6×6 lattice. It is obvious that the sharp peak at $(\pi, 0)/(0, \pi)$ persistently exists at various U and J , signifying a robust $(\pi, 0)/(0, \pi)$ magnetic order. In addition, such a stable spin order still persists on the 8×8 lattice [see Fig. 2(b)]. It is worth noting that the $(\pi, 0)/(0, \pi)$ peak in $S(k)$ can not be viewed as a criterion for the formation of the striped AFM order^{31,32}, as we will discuss later that another proposed magnetic order, the OM order³³, also has a similar magnetic structure.

In Fig. 1(a), we see that when increasing the Coulomb repulsion U , the magnetic order is enhanced. Since the strength of the Coulomb repulsion (in units of $|t_1|$) can be viewed as a measurement of the electronic correlation strength, such a U -induced enhancement implies the important role of electronic correlations for the investigated

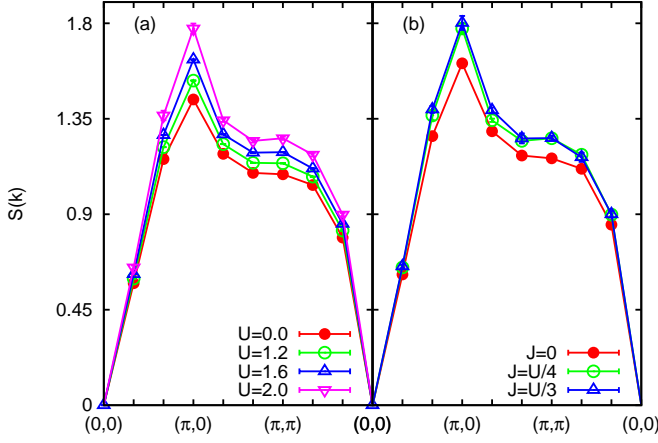


FIG. 1: (Color online) The static spin structure factor $S(k)$ at half filling on 6×6 cluster for (a) different on-site Coulomb repulsions U with fixed $J = 0.25U$ and (b) different Hund's couplings J with $U = 2.0$.

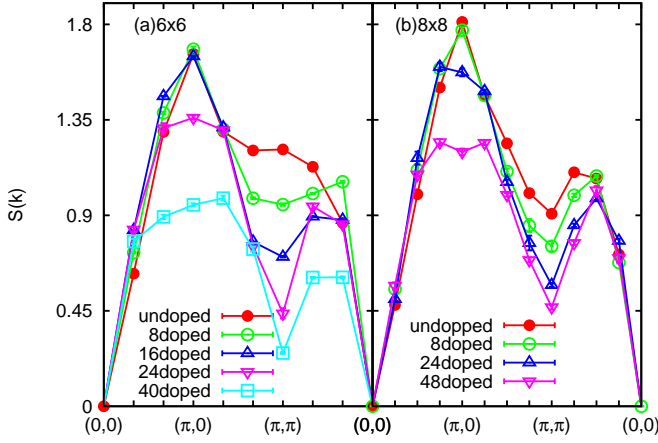


FIG. 2: (Color online) The effect of electron doping on the spin structure factor with $U = 1.4$, $J = 0.25U$ on (a) 6×6 and (b) 8×8 lattices. The integer before doped denotes the number of doped electrons.

magnetic order. Similarly, an enhancement in the magnetic order is again observed when increasing the Hund's coupling J at fixed $U = 2.0$ [see Fig. 1(b)], considering that J favors the local magnetic moments, which also signals possible contributions of the local moments to this magnetic order. Within the same argument, the robust $(\pi, 0)/(0, \pi)$ peak at $U = 0.0$ [see Fig. 1(a)] indicates that the magnetic order does not only relate to the electronic correlations and local moments, but also to other factors, such as the FS nesting.

Next we discuss the doping effects on the magnetic order. Upon electron doping, as shown in Fig. 2(a), the $(\pi, 0)$ peak seems to be unaffected compared with the undoped case initially, but the values of $S(k)$ along the $(\pi, 0)-(0, 0)$ direction are strongly suppressed. As a re-

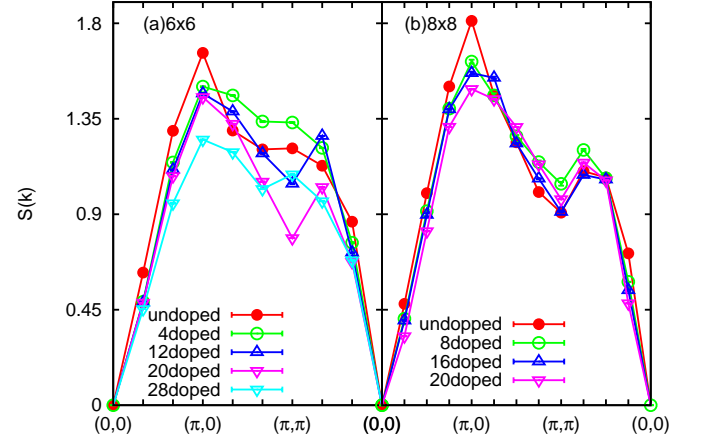


FIG. 3: (Color online) The effect of hole doping on the spin structure factor with $U = 1.4$, $J = 0.25U$ on (a) 6×6 and (b) 8×8 lattices. The integer before doped denotes the number of doped holes.

sult, the magnetic order is relatively enhanced. When more electrons are doped, the $(\pi, 0)$ point starts falling and a probable incommensurate $(\pi, 0)$ magnetic structure arises. Different from previous studies, we find that the effect of electron doping on the magnetic order is not a monotonic suppression and there may exist a small regime close to half filling where the magnetic order is enhanced or at least unaffected by doping. Similar phenomena are also observed on the 8×8 lattice as shown in Fig. 2(b).

In the hole-doped case, however, because of the particle-hole asymmetry of the two-orbital model, the behaviors of $S(k)$ with doping are different. In Fig. 3, the $(\pi, 0)$ peak is directly suppressed even at very low doping densities, and the values along with the $(\pi, \pi)-(0, 0)$ direction are relatively insensitive to the doping concentration. Interestingly, as reflected in Fig. 4, the different behaviors of the magnetic order for different dopants seem to be closely associated with their different FS evolutions upon doping: With exactly the same doping density, it is manifested that the electron pocket is notably diminished by hole doping while that of the electron-doped system is just slightly enlarged. On the other hand, in both cases the hole pockets almost remain unchanged. These facts may imply that the FS nesting remains in good condition at low electron doping while weakens at strong electron or hole dopings. This explains why the enhancement of magnetic order is observed only at low electron dopings. Therefore, we propose that at least in the intermediate interaction regime the FS nesting plays an important role in the magnetism of the two-orbital system.

Now we analyze the competing magnetic orders of the two-orbital model at half filling. As proposed in Ref. 33, the OM order, in which the magnetic moments on nearest-neighbor sites are at right angles, is recommended in the two-orbital model. Numerically, it is

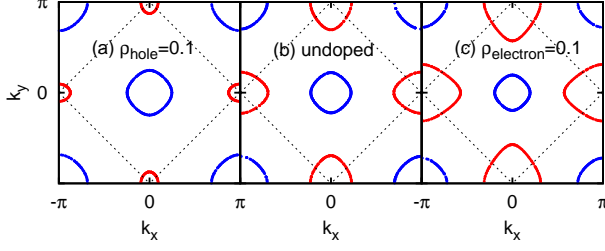


FIG. 4: (Color online) The Fermi surface in the extended Brillouin zone (1 Fe per unit cell) for (a) the hole-doped, (b) undoped, and (c) electron-doped systems with $U = 0.0$, $t_1 = -1.0$, $t_2 = 1.3$ and $t_3 = t_4 = -0.85$, where the dashed lines denote the folded Brillouin zone (2 Fe per cell) and the red (blue) curves represent the electron (hole) Fermi pockets.

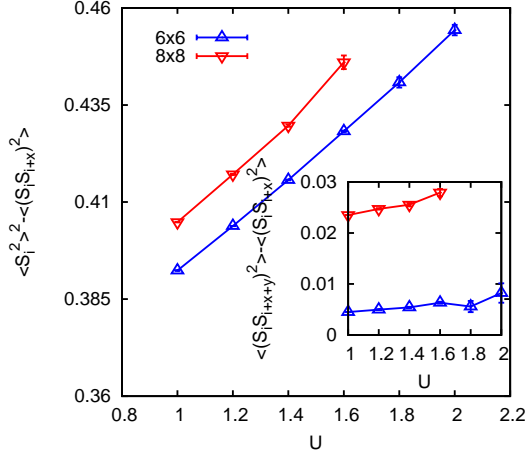


FIG. 5: (Color online) $\langle \vec{S}_i^2 \rangle^2 - \langle (\vec{S}_i \cdot \vec{S}_{i+\hat{x}})^2 \rangle$ versus Coulomb repulsion U on 6×6 and 8×8 lattice with $J = 0.25U$ at half filling. In order to further confirm the magnetic order, the dependence of $\langle (\vec{S}_i \cdot \vec{S}_{i+\hat{x}+\hat{y}})^2 \rangle - \langle (\vec{S}_i \cdot \vec{S}_{i+\hat{x}})^2 \rangle$ on U is illustrated in the inset.

rather difficult to distinguish the striped AFM and the OM order: both of them have similar magnetic structure factors, negative next-nearest-neighbor spin-spin correlations and almost-zero expectations of the nearest-neighbor spin-spin correlations⁶. In order to identify the competing magnetic orders at half filling, we calculate the expectation values of the four-spin-operator $\langle (\vec{S}_i \cdot \vec{S}_{i+\hat{x}})^2 \rangle$. If U favors the OM order, $\langle (\vec{S}_i \cdot \vec{S}_{i+\hat{x}})^2 \rangle$ should grow slower than $\langle \vec{S}_i^2 \rangle^2$. As a result, $\langle \vec{S}_i^2 \rangle^2 - \langle (\vec{S}_i \cdot \vec{S}_{i+\hat{x}})^2 \rangle$ should increase when increasing U . In Fig. 5, a clear U -dependent enhancement of $\langle \vec{S}_i^2 \rangle^2 - \langle (\vec{S}_i \cdot \vec{S}_{i+\hat{x}})^2 \rangle$ is observed on both 6×6 and 8×8 lattices, which implies a strong tendency for the formation of the OM order as U is increased. In addition, such a tendency becomes stronger when the lattice size is enlarged from 6×6 to 8×8 .

To substantiate this argument, we also calculate $\langle (\vec{S}_i \cdot \vec{S}_{i+\hat{x}+\hat{y}})^2 \rangle - \langle (\vec{S}_i \cdot \vec{S}_{i+\hat{x}})^2 \rangle$. Similarly, if U is in favor of

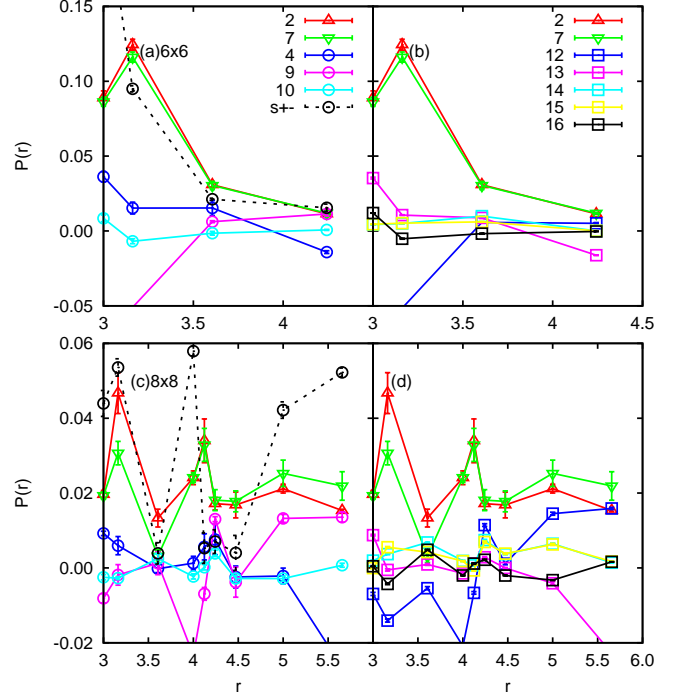


FIG. 6: (Color online) The non-on-site pairing correlations $P(r)$ as functions of the pairing distance r in electron-doped case. (a) and (c): The intraband singlet pairings 2, 7 v.s. all the interband singlet pairings on 6×6 and 8×8 lattices, respectively; (b) and (d): the intraband singlet pairings 2, 7 v.s. all the triplet pairings on the same lattices. The dashed line represents a nodeless s_{\pm} pairing discussed in the context. Here, 8 electrons are doped in the 6×6 and 8×8 lattices with $U = 1.4$, $J = 0.25U$.

the OM order, the nearest-neighbor spin-spin correlation ought to grow slower than the next-nearest-neighbor one. Then, $\langle (\vec{S}_i \cdot \vec{S}_{i+\hat{x}+\hat{y}})^2 \rangle - \langle (\vec{S}_i \cdot \vec{S}_{i+\hat{x}})^2 \rangle$ should also be enhanced by U , which is demonstrated by the results presented in the inset of Fig. 5.

From the above discussions, we conclude that at least in the weak to intermediate electronic correlation regime, the magnetic order at half filling in the two-orbital model tends to be in the OM order. Similar conclusions are drawn from the unrestricted Hartree-Fock³³ and DMRG¹⁶ studies of the same model on other lattices.

B. Pairing symmetry

Since the pairing symmetry is intricately related to the pairing mechanism, it is essential to clarify the dominant pairing channel among all the possible candidates. In this section, the long-range pairing correlations of the possible nearest-neighbor-bond pairing states²⁹ and a proposed nodeless s_{\pm} pairing state^{6,15} are discussed (see Table. I), and subsequently, the effects of the doping density ρ and

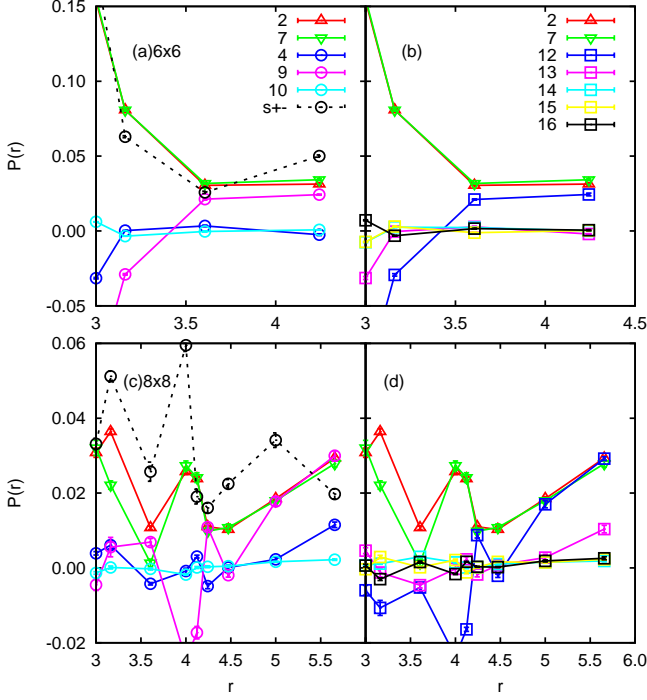


FIG. 7: (Color online) The non-on-site pairing correlations $P(r)$ as functions of the pairing distance r in hole-doped case. (a) and (c): The intraband singlet pairings 2, 7 v.s. all the interband singlet pairings; (b) and (d): the intraband singlet pairing 2,7 v.s. all the triplet pairings. Similar as in Fig. 6, the dash line represents the s_{\pm} pairing. In this case, 4 holes are doped in the 6×6 lattice and 8 holes in the 8×8 lattices with $U = 1.4$, $J = 0.25U$.

Coulomb repulsion U on the proposed pairing candidates are examined.

In Figs. 6(a) and 6(b), the pairing correlations of possible nearest-neighbor-bond pairings are shown as a function of pairing distance r when 8 electrons are doped into the 6×6 system. The pairings 2 and 7, which correspond to the spin singlet A_{1g} and B_{1g} intraband pairings, have the strongest amplitude at long distances. To see more clearly, all the singlet interband and triplet pairings are compared with pairings 2 and 7 in separated panels (a) and (b). Since the importance of the nodeless s_{\pm} pairing with a next-nearest-neighbor-bond pairing^{6,15}, we also show the corresponding pairing correlation in Fig. 6(a). The s_{\pm} pairing also has strong long-range pairing correlations, sometimes even stronger than that of pairings 2 and 7. The dominance of the three competing pairings are also revealed on the 8×8 lattice [see Figs. 6(c) and 6(d)].

In the hole-doped case (see Fig. 7), similar phenomena are observed on both 6×6 and 8×8 lattices. Remarkably, from Figs. 6 and 7, we find that the degeneracy not only occurs between pairings 2 and 7, but also among other pairings. For example, the singlet interband pairing 4

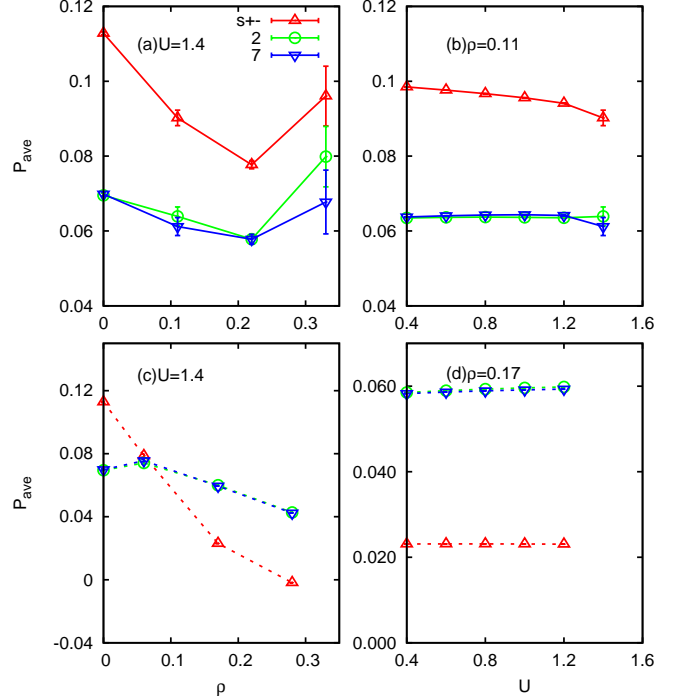


FIG. 8: (Color online) The average of long-range pairing correlation P_{ave} of 2, 7, and s_{\pm} as functions of the doping density ρ (a) and (c), and the Coulomb repulsion U (b) and (d) on the 6×6 lattice. (a) and (b) correspond to the electron-doped cases and (c) and (d) the hole-doped cases. Here, 8 electrons are doped in (b) and 4 holes in (d).

with A_{2g} symmetry almost has the same behaviors as the triplet pairing 13 with B_{2g} symmetry; the singlet B_{2g} interband pairing 9 also competes with the A_{2g} triplet pairing 12, and so on.

To illustrate the effect of doping density ρ and Coulomb repulsion U on the proposed pairing channels, the average of long-range pairing correlation, $P_{ave} = \frac{1}{M} \sum_{r>3} P(r)$ with M the number of pairs, is plotted in Fig. 8 as functions of ρ and U for electron- and hole-doped cases. From Figs. 8(a) and 8(c), we observe that in both the electron- and hole-doped cases, the s_{\pm} pairing, together with pairing 2 and 7, are suppressed when increasing the doping density ρ . Obviously, the s_{\pm} pairing is dominant in the electron-doped case, whereas in the hole-doped case the suppression of the s_{\pm} pairing is more drastic than that of the pairing 2 and 7, and in contrary to the electron-doped case, the pairings 2 and 7 become the dominant ones when $\rho > 0.06$.

Lastly, with a fixed doping density ρ , we study the effect of the Coulomb repulsion U on the pairing correlations, as presented in Figs. 8(b) and 8(d). Overall, the effect of U is much weaker than that of doping—the pairing properties are almost unchanged when U is increased. In consistent with Figs. 8 (a) and 8(c), the s_{\pm} pairing prevails over the pairings 2 and 7 in the electron-doped

case, and the latter become the leading channels in hole doping. Thus our results demonstrate dopant-dependent pairing symmetries of the two-orbital model.

IV. CONCLUSIONS

In this paper, we have systematically studied the magnetic and pairing properties of the two-orbital model for pnictides at half filling and in electron- and hole-doped cases. We found that the $(\pi, 0)/(0, \pi)$ magnetic order is robust at half filling in the weak to intermediate interaction regime. When increasing the Coulomb repulsion U , the magnetic order is enhanced and the system tends to be in the OM order, which is consistent with the unrestricted Hartree-Fock and DMRG studies.^{16,33}

When the system is doped away from half filling, the magnetic order has different behaviors in the electron and hole dopings: It is relatively enhanced upon the electron doping and suppressed eventually; while in the hole-doped case, the magnetic order is directly suppressed. Such a difference is closely relevant to different evolu-

tions of the FS when electrons and holes are doped in the system—the FS nesting remains in good condition in the light electron doping while in the hole-doped case, the electron pocket is significantly shrunk and thus the nesting can hardly be realized.

The strong doping effects on the long-range pairing correlations were also observed in the two-orbital model. In electron-doped case, an s_{\pm} pairing state dominates the possible nearest-neighbor-bond pairing channels, while two nearly degenerate intraband singlet pairing channels with A_{1g} and B_{1g} symmetries take over in the hole-doped case, which illustrates a dopant-dependent pairing property of the two-orbital model.

Acknowledgments

The authors thank Adriana Moreo for useful discussions. This work was supported by NSFC under Grants Nos. 11174072 and 91221103, and by SRDP under Grant No. 20104208110001.

-
- * Electronic address: gkliu@mail.bnu.edu.cn
 - † Electronic address: huangzb@hubu.edu.cn
 - ‡ Electronic address: yjwang@bnu.edu.cn
 - ¹ V. Vildosola, L. Pourovskii, R. Arita, S. Biermann, and A. Georges, Phys. Rev. B **78**, 064518 (2008).
 - ² I. I. Mazin, D. J. Singh, M. D. Johannes, and M. H. Du, Phys. Rev. Lett. **101**, 057003 (2008).
 - ³ S. Raghu, X.-L. Qi, C.-X. Liu, D. J. Scalapino, and S.-C. Zhang, Phys. Rev. B **77**, 220503 (2008).
 - ⁴ M. Daghofer, A. Nicholson, A. Moreo, and E. Dagotto, Phys. Rev. B **81**, 014511 (2010).
 - ⁵ K. Kuroki, S. Onari, R. Arita, H. Usui, Y. Tanaka, H. Kon-tani, and H. Aoki, Phys. Rev. Lett. **101**, 087004 (2008).
 - ⁶ A. Moreo, M. Daghofer, J. Riera, and E. Dagotto, Phys. Rev. B **79**, 134502 (2009).
 - ⁷ J. Hu and N. Hao, Phys. Rev. X **2**, 021009 (2012).
 - ⁸ S. Graser, T. A. Maier, P. J. Hirschfeld, and D. J. Scalapino, New Journal of Physics **11**, 025016 (2009).
 - ⁹ X.-L. Qi, S. Raghu, C.-X. Liu, D. J. Scalapino, and S.-C. Zhang (2008), arXiv: 0804.4332v2.
 - ¹⁰ Y. Bang, Phys. Rev. B **78**, 134523 (2008).
 - ¹¹ Z.-J. Yao, J.-X. Li, and Z. D. Wang, New Journal of Physics **11**, 025009 (2009).
 - ¹² F. Wang, H. Zhai, Y. Ran, A. Vishwanath, and D.-H. Lee (2008), arXiv:0805.3343v3.
 - ¹³ X. Dai, Z. Fang, Y. Zhou, and F.-C. Zhang, Phys. Rev. Lett. **101**, 057008 (2008).
 - ¹⁴ M. Daghofer, A. Moreo, J. Riera, E. Arrigoni, D. Scalapino, and E. Dagotto, Phys. Rev. Lett. **101**, 237004 (2008).
 - ¹⁵ A. Nicholson, W. Ge, X. Zhang, J. Riera, M. Daghofer, A. M. Oleś, G. B. Martins, A. Moreo, and E. Dagotto, Phys. Rev. Lett. **106**, 217002 (2011).
 - ¹⁶ E. Berg, S. A. Kivelson, and D. J. Scalapino, Phys. Rev. B **81**, 172504 (2010).
 - ¹⁷ K. Held and D. Vollhardt, The European Physical Journal B-Condensed Matter and Complex Systems **5**, 473 (1998).
 - ¹⁸ S. Sakai, R. Arita, and H. Aoki, Phys. Rev. B **70**, 172504 (2004).
 - ¹⁹ J. E. Hirsch, Phys. Rev. B **28**, 4059 (1983).
 - ²⁰ S. Zhang, J. Carlson, and J. E. Gubernatis, Phys. Rev. B **55**, 7464 (1997).
 - ²¹ D. J. Singh and M.-H. Du, Phys. Rev. Lett. **100**, 237003 (2008).
 - ²² G. Xu, W. Ming, Y. Yao, X. Dai, S.-C. Zhang, and Z. Fang, EPL (Europhysics Letters) **82**, 67002 (2008), ISSN 0295-5075.
 - ²³ E. Bascones, M. J. Calderón, and B. Valenzuela, Phys. Rev. Lett. **104**, 227201 (2010), ISSN 0031-9007.
 - ²⁴ Q. Luo, G. Martins, D.-X. Yao, M. Daghofer, R. Yu, A. Moreo, and E. Dagotto, Phys. Rev. B **82**, 104508 (2010).
 - ²⁵ E. Dagotto, T. Hotta, and A. Moreo, Physics Reports **344**, 1 (2001).
 - ²⁶ P. Dai, J. Hu, and E. Dagotto, Nature Physics **8**, 709 (2012), ISSN 1745-2473.
 - ²⁷ S. R. White, D. J. Scalapino, R. L. Sugar, E. Y. Loh, J. E. Gubernatis, and R. T. Scalettar, Phys. Rev. B **40**, 506 (1989).
 - ²⁸ W. Hanke and Y. Kopaev, *Chapter 3, Electronic phase transitions*, Modern problems in condensed matter sciences (North-Holland, 1992).
 - ²⁹ Y. Wan and Q.-H. Wang, EPL (Europhysics Letters) **85**, 57007 (2009), ISSN 0295-5075.
 - ³⁰ A. Moreo, M. Daghofer, A. Nicholson, and E. Dagotto, Phys. Rev. B **80**, 104507 (2009).
 - ³¹ J. Dong, H. J. Zhang, G. Xu, Z. Li, G. Li, W. Z. Hu, D. Wu, G. F. Chen, X. Dai, J. L. Luo, et al., EPL (Europhysics Letters) **83**, 27006 (2008).
 - ³² J. Paglione and R. L. Greene, Nature Physics **6**, 645

- (2010).
- ³³ J. Lorenzana, G. Seibold, C. Ortix, and M. Grilli, Phys. Rev. Lett. **101**, 186402 (2008).